An Evaluation of Electrical Resistivity Tomography for Stratigraphic Characterization of Paleochannels at the Hanford Site – 21024

Judy Robinson*, Jonathan Thomle*, Mark Rockhold*, Timothy Johnson*, Vicky Freedman*
* Pacific Northwest National Laboratory, Richland, Washington

ABSTRACT

Paleochannels in the subsurface can act as preferential contaminant transport pathways and shorten travel times to downstream receptors. At the Hanford Site in Washington State (USA), a paleochannel of more permeable material has been inferred to exist within the Central Plateau between the Hanford 200 Areas at a depth of ~80 m below the ground surface. This inference is based on concentrations measured at monitoring wells and sparse borehole information. Because the extent of the paleochannel will strongly influence contaminant transport to downstream receptors and the Columbia River, a more accurate delineation of the paleochannel can guide placement of future borehole locations used for characterizing the geologic conceptual model, and for contaminant transport predictions. To this end, the feasibility of electrical resistivity tomography (ERT) has been evaluated to help delineate preferential flow paths between the 200 Areas.

A numerical assessment preceded field work to evaluate ERT, coupling flow and transport simulations with ERT. The numerical evaluation first examined 1) the electrical conductivity (EC) contrast based on lithology using static imaging and 2) the EC contrast based on a potential high ionic strength tracer injection in groundwater. Static ERT imaging simulations showed higher horizontal resolution relative to the vertical, and vertical contacts of the paleochannel were identified. Tracer injection simulations showed that high tracer concentrations were required to detect its transport through the paleochannel, with transport times on the order of decades.

A limited field campaign was conducted between the 200 Areas to assess data quality, depth of investigation, and signal strength. A two-dimensional (2D) surface ERT field survey was conducted along a 1.6-km array using 64 electrodes spaced 25 m apart and with four different electrode configurations. 2D ERT imaging detected two low electrically conductive regions and confirmed limited vertical compared to horizontal resolution identified in the numerical modeling. The locations of the two low electrically conductive regions were inferred to be the coarser paleochannel sediments. Additional 2D surface ERT surveys are planned to further delineate the high-permeability channel. Significant cost savings are anticipated using ERT to delineate subsurface stratigraphy and to optimize the use of other, more expensive site characterization technologies, such as borehole drilling.

INTRODUCTION

Paleochannels at the Hanford Site in Washington State (USA) are large features, often kilometers wide, that are difficult to map using borehole data. This is especially true between the Hanford 200 Areas, where a paleochannel has been inferred ~80 m below the ground surface from monitoring wells and sparse borehole information. Efficient tools are needed to guide placement of characterization boreholes. The geophysical method electrical resistivity tomography (ERT) was evaluated as a method to help delineate preferential flow paths between the 200 Areas.

ERT can provide information at large spatial scales. ERT provides a distribution of bulk electrical conductivity (EC), which is dependent on physical properties such as lithology, pore water fluid conductivity, porosity, moisture content, and temperature. [1] The contrast in these physical properties affects the measurement of bulk EC. Depending on the ERT survey needs, the spacing and number of ERT sensors can be adjusted. Increasing the spacing between ERT sensors allows for deeper distance penetration, but at a decreased resolution.

Within the Hanford 300 Area, extensive ERT field work has been performed to locate paleochannels along and adjacent to the Columbia River to identify uranium transport pathways. These features, identified as coarse-grained Hanford sediments incised into finer-grained Ringold Formation sediments, were found to play an important role in surface water-groundwater exchange. After identification of the Hanford-Ringold contact [2], time-lapse ERT imaging was focused near the deepest contact location using the Columbia River water as a tracer to detect river water incursion patterns [3]. Inland time-lapse dynamics in the 300 Area were examined using 2D ERT by [4] and three-dimensional (3D) ERT by [5]. These studies demonstrated the viability of static and time-lapse surface ERT imaging at Hanford for paleochannel mapping, providing one basis for examining ERT to delineate preferential flow paths between the 200 Areas.

In this work, numerical simulations preceded a field assessment whereby a flow and transport simulator was used to generate data on conceptual site models used to evaluate 3D ERT. The numerical evaluation first examined 1) the EC contrast based on lithology using static imaging and 2) the EC contrast based on a potential high ionic strength tracer injection in groundwater. The latter scenario increases the electrical conductivity contrast and could therefore be used to image spatial and temporal changes in EC based on the tracer transport through the higher conductivity sediments. Uncertainty was explored in these simulations by varying the ERT survey design, petrophysical parameters, and the tracer volume and concentrations.

A 2D field campaign was conducted between the 200 East and West Areas to assess data quality, depth of investigation, and signal strength. The 2D surface ERT field survey was conducted along a 1.6-km array using 64 electrodes spaced 25 m apart. Four different electrode configurations were used to assess strengths and weaknesses during static imaging with widely spaced dipoles. The 2D surface ERT results are compared to the findings of the numerical simulations and the current geologic framework between the 200 Areas.

Numerical simulations and a limited field campaign provide the strategic decision-making tools to determine feasibility of mapping of large-scale paleochannels and locating future monitoring wells between the 200 East and West Areas with ERT. Significant cost savings are anticipated using ERT to delineate subsurface stratigraphy and to optimize the use of other, more expensive site characterization technologies, such as borehole drilling.

Site description

The ERT feasibility study was conducted near the inferred location of a paleochannel between the 200 East and West Areas on the Central Plateau at the Hanford Site (Fig. 1). The 2D field ERT line is shown in orange and runs from northeast to southwest. This line crosses the inferred paleochannel boundary at two locations. The 3D numerical ERT study electrode locations (192 total) are shown in white. There are two candidate tracer injection wells, designated as 699-49-69 and MW-10A, which were used for the tracer injection simulations. Well 699-49-69 is currently being used as an injection well for an existing pump-and-treat system and is located outside of the inferred paleochannel. Well MW-10A is located within the paleochannel and has been proposed as a groundwater monitoring well, presumed for these simulations to be screened at the depth of groundwater. Well 699-46-68 is shown along the 2D ERT field line. This well has a metallic casing and was included in the 2D ERT field modeling.

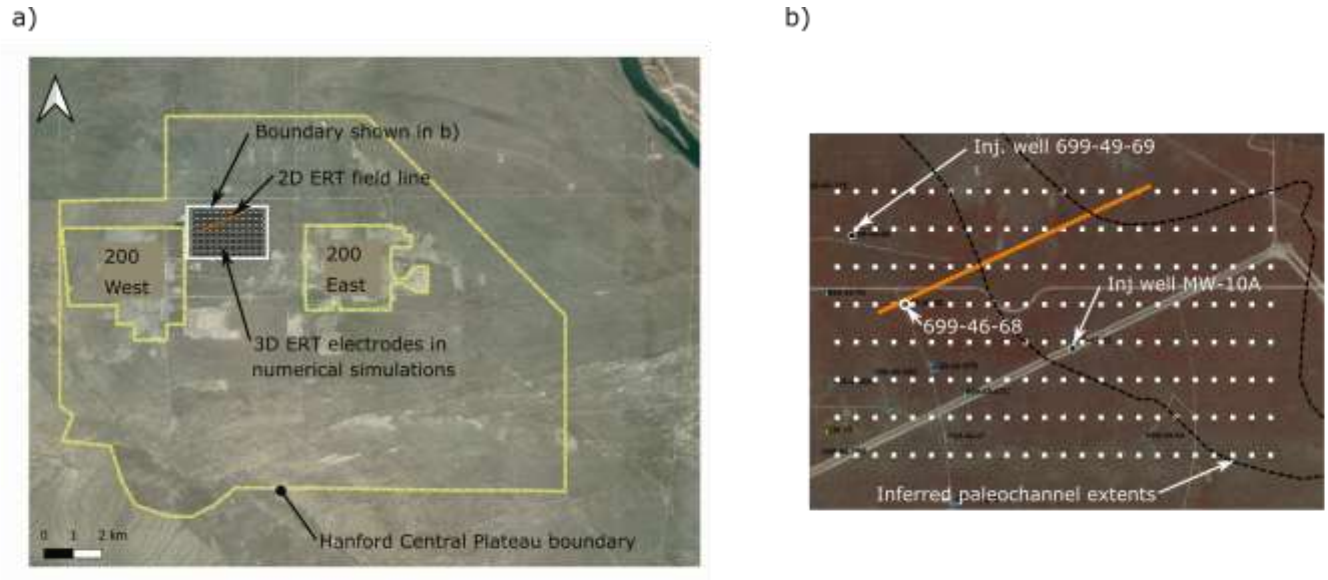

Fig. 1. Layout of Electrodes for 3D ERT Numerical Simulations and 2D ERT Field Line. Electrodes for the 3D ERT numerical simulation are shown in white. Field electrode locations for the 2D ERT line are shown in orange. Tracer injection wells 699-49-69 and MW-10A used in the 3D ERT numerical simulations are shown as are the inferred paleochannel extents from the geologic framework model. Well 699-46-68, which has a metallic casing, is shown along the 2D ERT field line and was included in the field ERT modeling.

METHODS

Simulations of groundwater flow and solute transport were performed using the water operational mode of eSTOMP [6], a parallel version of STOMP [7]. ERT imaging simulations and field data inverse modeling were conducted using E4D, an open source 3D modeling and inversion code designed to run on distributed memory parallel computing systems. [https://e4d-userguide.pnnl.gov/, 8,9]

3D numerical simulations

The 3D numerical simulations provided information on porosity and saturation that were converted into bulk ECs. ERT modeling was then used to simulate transfer resistance data and to image the subsurface. Results were then compared to the groundwater model. The eSTOMP simulator uses a 3D structured grid with orthogonal, hexahedral grid blocks, while E4D discretizes the model space with a 3D unstructured tetrahedral mesh. Therefore, eSTOMP output was interpolated to the E4D mesh using the mesh interpolation scheme of Johnson et al (2017). [10]

Flow and transport simulations

The flow and transport simulations used the Central Plateau Vadose Zone Geoframework model (GFM) ([11-13]) as a geologic framework and the calibrated Plateau-to-River (P2R) model described by Budge 2019 for elevations below 140 m. [14] The sensitivity of ERT predictions to uncertainties in vadose zone hydrologic parameters was considered in these simulations. Physical and hydraulic properties were based on three different sets of parameters derived from 1) vadose zone sediments in the Hanford WA-1 waste management area (as used in Robinson et al (2020)); 2) two generic vadose zone geologic frameworks based on Last et al (2006). [15,16] Other variations on input variables to the eSTOMP modeling included the tracer volume and concentration. The tracer was assumed to be potassium bromide (KBr).

Petrophysical transformation

eSTOMP outputs parameters of interconnected porosity ϕ_{int} and aqueous saturation S and tracer (KBr) concentrations that are transformed into bulk EC σ for the ERT simulations. For a partially saturated electrically resistive sediment, Archie's law describes the relationship between bulk EC σ and pore space properties as

$$\sigma = \sigma_w \phi_{int}^m S^n \qquad \text{(Eq. 1)}$$

where σ_w is the fluid conductivity and ϕ_{int} is the interconnected porosity.[17] Note that surface conduction is neglected in Eq. **Error! Reference source not found.**, which is valid to a first-order, given that the target zones are permeable buried features with coarser sediments. The cementation exponent m is a function of the rate of change in pore complexity with porosity [18], dependent on particle shape and orientation [19], and typically varies between 1.2 and 4.4 [20]. Numerical simulations considered values of m equal to 1.3 (e.g., Robinson et al 2020) and 1.8 to compare the effects on the ERT imaging and evaluate uncertainty in petrophysical parameters. [21] The saturation exponent n is associated with the additional tortuosity due to the replacement of pore fluid with air (an insulator). Commonly, n = 2 is used and was also assumed in this assessment. [22, 23]

ERT simulations

The ERT electrodes (24x8=192 total) were spaced 100 m apart in an east/west direction and 200 m apart in a north/south direction. Prior to the tracer injection, a synthetic background characterization dataset was inverted to determine if the conductivity structure could delineate lithologic boundaries at and below the water table. Time-lapse ERT simulations began after the tracer injections and used the background conductivity as the starting model. Changes from the background model were inverted within the region below the water table. This assumes there were no site activities that would produce changes in conductivity within the vadose zone that would affect the saturated zone, which is justified at this scale assuming annual recharge remains relatively constant. [24]

Two hypothetical 3D ERT surveys were considered. The first consisted of 2828 focused (F) four-electrode measurements. This configuration collected data where current and potential electrodes all fall in the same row or column (refer to Fig. 1). The second survey contained 21,822 measurements consisting of Wenner, Schlumberger, and dipole-dipole comprehensive (C) measurements. Noise added to the synthetic datasets (and used in the inversion modeling) was 2% with an absolute error of 0.001 ohms. [25] Additional measurements have the potential to provide more information on the subsurface, particularly for background/characterization imaging. However, more measurements translates to increased computational time. A summary of 3D ERT coupled numerical simulations is provided in TABLE I.

TABLE I. Conceptualizations Used in ERT Feasibility Evaluation

Tracer Volume	**378 m^3**	**757 m^3**												**1135 m^3**
Archie's Petrophysical Parameters	*m*=1.3 *n*=2	*m*=1.3 *n*=2						*m*=1.8 *n*=2						*m*=1.3 *n*=2
Tracer (KBr) Concentration	60 g/L	40 g/L		60 g/L		80 g/L		40 g/L		60 g/L		80 g/L		60 g/L
ERT Survey	F	F	C	F	C	F	C	F	C	F	C	F	C	F

F=Focused survey, contains 2828 measurements.
C=Comprehensive survey, contains 21,822 measurements.

2D field study

The 2D ERT surface electrode array was designed to image the subsurface down to roughly 120 m elevation (Fig. 2). A total of 64 electrodes, spaced approximately 25 m apart, were installed for a total line length of approximately 1575 m (Fig. 1). The electrodes are 10-inch-long galvanized carbon steel spikes. Four electrodes act collectively as one current injection location (Fig. 2b). The electrodes were installed manually using hand tools through four 1/2-inch-diameter holes in an electrical isolation box (Fig. 2b). A Multi-Phase Technologies (model MPT-DAS1) ERT system was used (Fig. 2c).

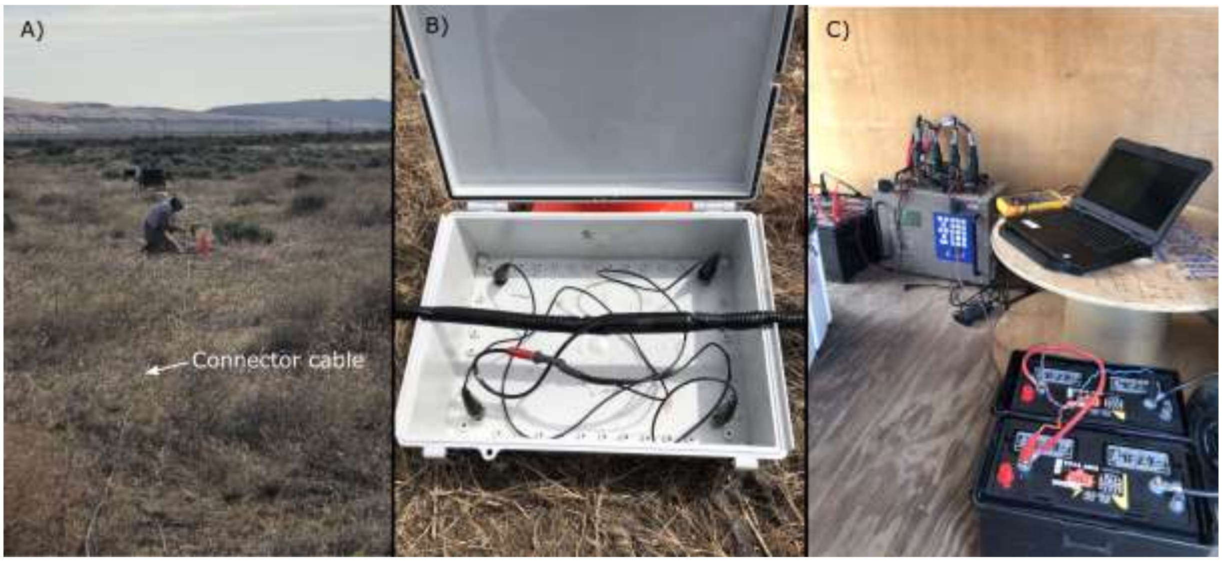

Fig. 2. Field Site Data Collection Images: A) representative field site image showing installation of electrodes; B) electrode isolation box containing connector cable and ERT hookups with four electrodes penetrating to the surface; C) MPT-DAS1 system for field data collection.

ERT measurements included a comprehensive series of Wenner-Alpha, Schlumberger, multiple-gradient, and dipole-dipole four-electrode configurations. Small-offset dipoles (electrodes pairs near each other) provide high resolution near the electrodes and constrain near-surface structures in the ERT inversion. Large offset dipoles probe deeper into the subsurface. The comprehensive combination of small, intermediate, and large offset dipoles used in the survey was implemented to provide optimal resolution for both shallow and deep structures to the extent possible. The survey was also optimized to leverage the eight channels available in the MPT-DAS 1 system; eight different potential electrode pairs were recorded for each current electrode pair. In total, 6,500 measurements were collected.

Electrical current flow can be impacted by topography and metallic infrastructure. To avoid inaccuracies in the ERT modeling, site lidar data at 15-m resolution was incorporated in the surface representation of the site. In addition, interference from a single metallic cased well (see Fig. 1b, well 699-46-68) was removed from the ERT modeling. [26]

Data quality was assessed by reviewing contact resistances, current injections, and stacking deviations for each measurement. Using conservative boundaries for these values, outlier measurements were removed. The total number of outliers was 8% of the data collected, confirming that the dataset is of very high quality. Data quality was also assessed through collection of full set of reciprocal measurements. This is where the current and potential electrode pairs are swapped in the measurements. In theory, the normal and reciprocal measurement should be equal and differences can be attributed to data noise. [27] Reciprocal error R_e in units of ohm is defined as:

$$R_e = |R_N - R_R|, \quad \text{(Eq. 2)}$$

where R_N is the measured normal resistance and R_R is the measured reciprocal resistance. The signal-to-noise ratio (SNR) reciprocal error is defined as:

$$\frac{|R_{avg}|}{R_e}, \text{ where} \quad \text{(Eq. 3)}$$

$$R_{avg} = (R_N + R_R)/2 \quad \text{(Eq. 4)}$$

The SNR was used to assess data quality from the 2D ERT field survey.

RESULTS

3D numerical simulations

Static imaging

The main findings of the simulations are shown as a subset of the simulations in TABLE I for brevity. The background ERT simulations, which are representative of static ERT imaging before a tracer is injected, are shown in Fig. 3. The top images represent the bulk EC models derived from the petrophysical transformation (using Eq. 1) of eSTOMP flow model parameters. These bulk EC models were used to generate synthetic ERT datasets using the comprehensive (21,822 measurements) survey. Two values of m, 1.3 and 1.8, are used, which produce different bulk EC models by which to evaluate ERT. The bottom images represent the inverted synthetic ERT datasets from these models. The impact of varying m is evident and clearly affects the ability of ERT to resolve subsurface structure. Generally, horizontal resolution is higher than vertical resolution. Horizontal contacts (vertical resolution) are better delineated where there are higher ECs (as shown in Fig. 3C).

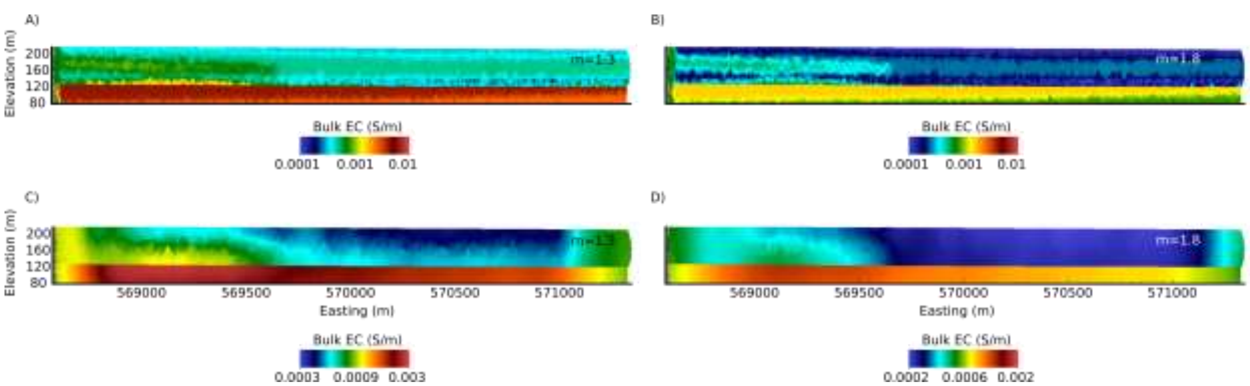

Fig. 3. Bulk EC Shown for the Comprehensive Survey. Flow and transport σ (from Eq. 1) are shown for A) m=1.3 and B) m=1.8. Inverted ERT modeling results are shown in C) and D). Cross section is oriented east/west through the center of the ERT grid.

Fig. 4 compares simulation results obtained using comprehensive (21,822 measurements) and focused (2,828 measurements) ERT surveys. While the comprehensive survey has a finer resolution, the impact to the overall EC structure interpretation is marginal, even though the number of measurements in the focused survey is about 13% of comprehensive survey. ERT survey optimization is an active area of research, and this study demonstrates that it is possible to reduce field data acquisition times (and processing); however, sites should be evaluated on a case-by-case basis. Given these results, time-lapse simulations used the focused (F) ERT survey.

Using these static numerical ERT simulations as a basis for field distributions of bulk EC, the contrast between sediments within and outside of the paleochannel varies by one order of magnitude or less. In addition, it was anticipated that horizontal resolution would exceed vertical resolution.

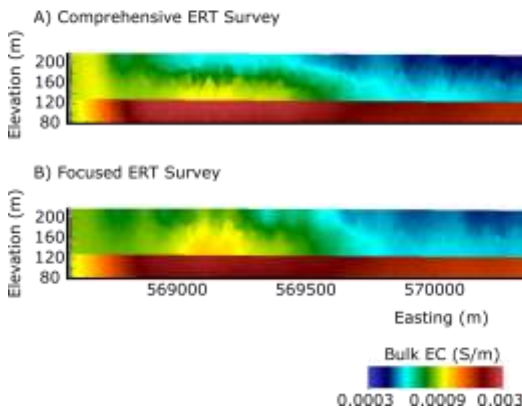

Fig. 4. ERT Bulk Imaging Results when Using A) Comprehensive Survey (C) versus B) Focused Survey (F)

Time-lapse imaging using a tracer injection

Tracer injections were simulated for a tracer volume of 757 m^3 and a tracer concentration of 60 g/L, as shown in Fig. 5. The flow and transport models predict high dilution over a long time period. The spatial extent of the tracer reaches a maximum during year 2028; however, most tracer concentrations are less than 1% of the injected concentration of 60 g/L. This has impacts for evaluating ERT feasibility, since in locations that have high dilution, the bulk EC contrast after the petrophysical transformation will not be large enough to be detected using ERT (Fig. 6).

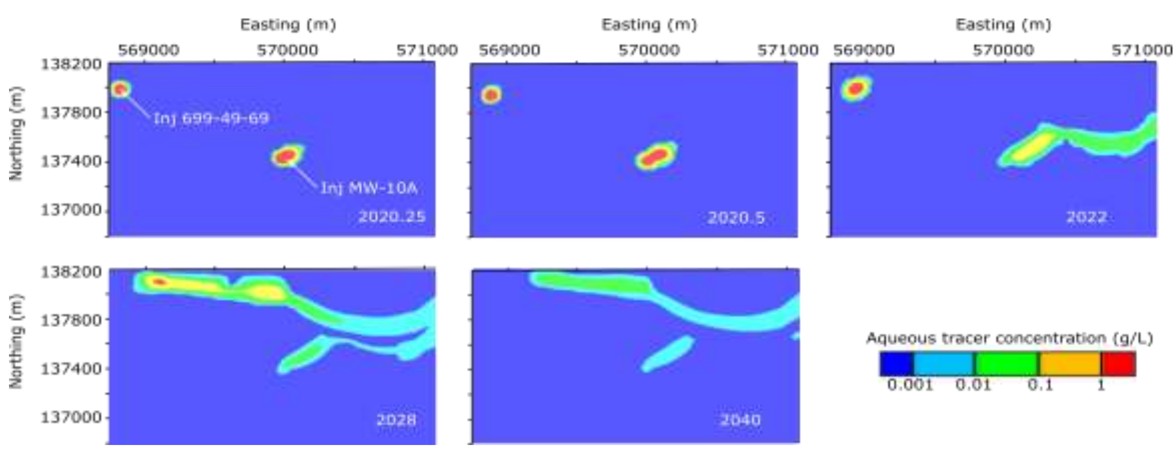

Fig. 5. eSTOMP Tracer Injection Models Shown at Elevation 120 m (top of water table) with a Tracer Volume of 757 m^3 and Tracer Concentration of 60 g/L

The bulk EC representations of Fig. 5 tracer concentrations after the petrophysical transformation (Eq. 1) are shown in Fig. 6 for three tracer volumes. The blue scale in these images represents the logarithmic change in bulk EC from the eSTOMP simulations before a tracer was injected. Therefore, the blue scale represents the true bulk EC contrast and the criteria by which the time-lapse ERT results should be evaluated. Comparing the spatial extents of the aqueous tracer concentrations (Fig. 5) to the bulk EC transformation (Fig. 6), it is evident that areas with low tracer concentrations do not increase the bulk EC. This limits the ability of ERT to image the full extent of the tracer in areas with low concentration.

The orange scale (Fig. 6) represents the ERT-detected tracer over time. For an injection volume of 378 m^3, ERT detection is minimal. The ERT detection increases for 757 m^3 and 1135 m^3; however, the low-conductivity tracer tail in the flow and transport bulk EC σ is not well resolved.

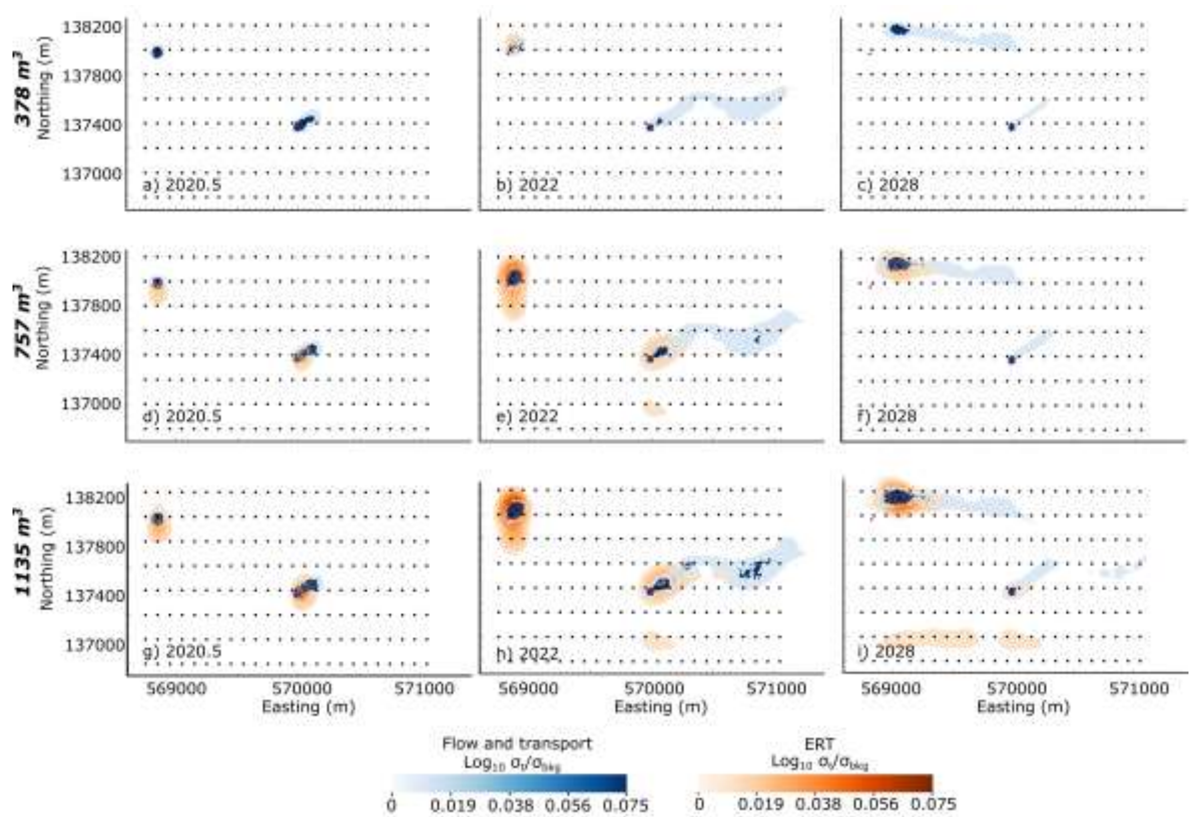

Fig. 6. Time Lapse ERT Simulation Results at Elevation 120 m using a 60 g/L Tracer Injection for Years 2020.5, 2022, and 2028 for Injection Volumes 378 m^3, 757 m^3, and 1135 m^3. The Archie's parameters used in the synthetic modeling were m=1.3 and n=2.

2D field study

For the field 2D ERT study, a comprehensive data quality evaluation based on reciprocity was conducted, which showed high SNRs (>300) regardless of electrode configuration type (TABLE II). The total number of measurements used in the ERT inversion was 5003. The raw ERT data was fit to the inverted ERT model with high fidelity. This requires high-quality data, accurate electrode locations, and accurate forward model simulations.

TABLE II. ERT Reciprocity Analysis

Electrode Configuration	**Total # Measurements**	**SNR**	**Inverted # Measurements**
Wenner-Schlumberger	1828	1333	1764
Multiple gradient	2072	714	1629
Dipole-dipole	2600	364	1610
Total	*6500*		*5003*

Fig. 7 shows the geologic framework model compared to the ERT model inversion results to potentially correlate these two disparate informational images. Well 699-46-68, which is offset from the ERT line, is also shown for reference. The x-axis denotes the length along the ERT line, starting from the southwestern-most electrode and ending at the northeastern-most electrode. The paleochannel location in Fig. 7A is presumed to be within the Hanford units (shown as a deep and mid-cyan color). A vertical boundary is shown within the Hanford unit between 550 and 600 m, which represents the location where a paleochannel feature is predicted.

Within the ERT image (Fig. 7B), coarser units are presumed to be zones of low EC above the water table, representing low-saturation units within the stratigraphic sequence. The shaded regions at depth represent poorly resolved zones identified through a sensitivity analysis following the approach of [28]. The image delineates two low EC features, with a higher EC feature in between. A near-surface high conductivity feature corresponds with the road crossing, potentially caused by backfill or road runoff events.

The geologic interpretation between 550 and 600 m does not correlate well with the ERT image, which is an area with sparse borehole coverage. This suggests ERT has delineated a subsurface structure that can be used to interpret the geologic conceptual model in areas with limited borehole information.

Note that below the water table, coarser paleochannel units are expected to have a higher (not lower) EC than surrounding units, however, as shown the lower conductivity features extend below the water table. The ERT data alone were not able to resolve the sharp conductivity contrast expected at the water table. E4D allows a sharp conductivity contrast to be imposed at the water table boundary; however, including this constraint did not change the horizontal boundaries of the paleochannel and added complexity (at this boundary) to the image. Therefore, results are shown without this constraint. The low EC regions in the vadose zone can be interpreted as zones where coarser sediments incise into lower units.

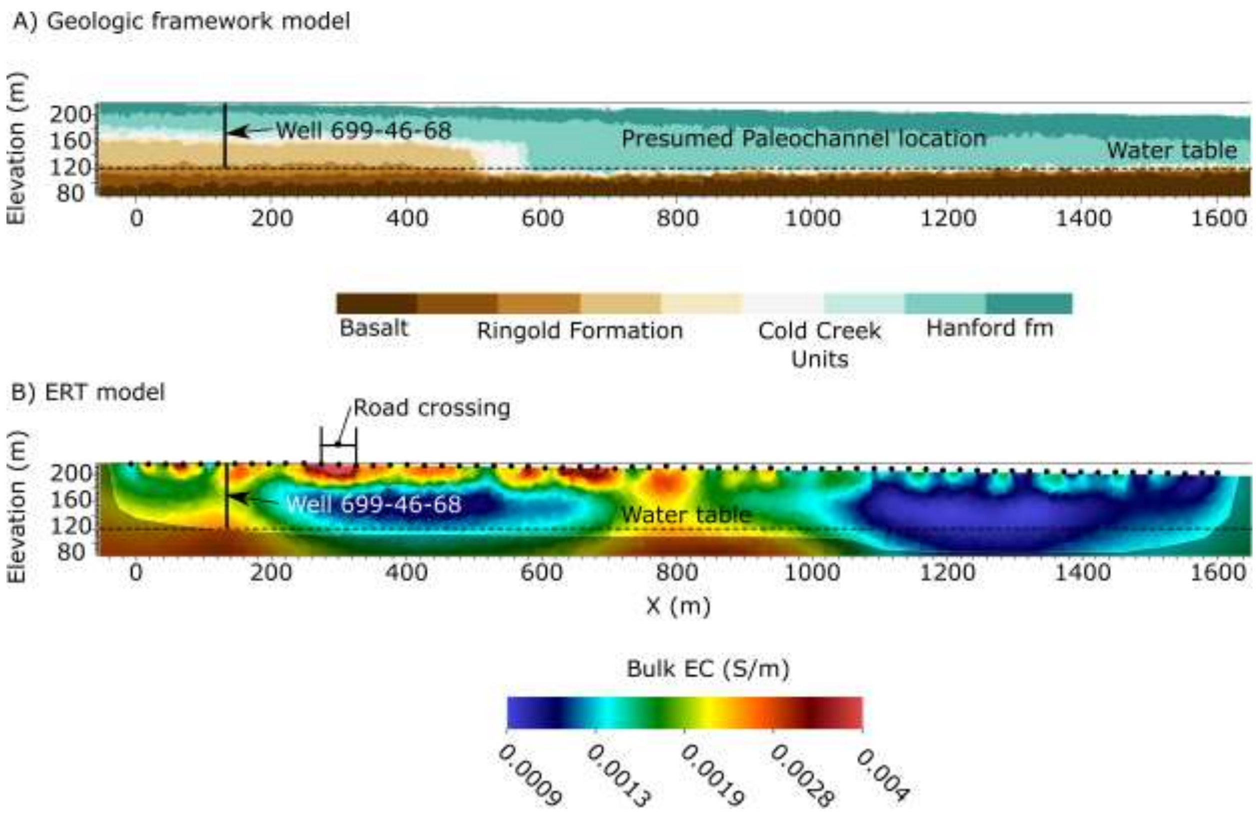

Fig. 7. A Comparison of A) the Geologic Framework Model Compared to B) the ERT Inversion Results. The shaded gray region at depth in B) represents poorly resolved ERT zones.

CONCLUSIONS

The coupled flow and transport and ERT simulations represent an evaluation of a large-scale ERT field survey with a tracer injection for paleochannel identification. The simulations allowed for realistic expectations for static and time-lapse ERT imaging prior to field imaging. The 2D ERT field survey provided an assessment of data quality/site noise, signal strength, and bulk EC structure. The bulk EC structure from the field survey was aligned with the findings for static ERT imaging in terms of bulk EC contrast and site noise levels.

Static 2D ERT imaging in the field delineated vertical contacts within the vadose zone. The depth of investigation was estimated to be below the water table. The presumption is that contrasting low electrically conductive features are representative of high hydraulic conductivity units incised into the deeper units and represent areas where there are likely highly transmissive units below the water table.

Additional 2D ERT static imaging is planned between 200 East and West to map areas where transmissive features extend below the water table. Combining 2D ERT static surveys allows for a pseudo-3D evaluation and interpretation between 200 West and East. Individual evaluation of each 2D dataset could potentially be used to determine subsequent locations. This overall could be an advantage for the kilometer-scale area between the 200 East and West Areas.

Data collection and analyses could be followed by a) selection of borehole locations within the paleochannel to confirm the interpretation of the ERT results and to monitor groundwater concentrations and/or b) refinement of the location of an ERT field campaign/feasibility using a tracer injection to monitor transport over time. The optimization provided by using ERT is expected to result in cost savings compared to other more expensive characterization options, such as borehole drilling.

REFERENCES

1. A. BINLEY, "Tools and Techniques: Electrical Methods," *Treatise on Geophysics*, 233-259 (2015). https://doi.org/10.1016/B978-0-444-53802-4.00192-5
2. L. D. SLATER, D. NTARLAGIANNIS, F. D. DAY-LEWIS, K. MWAKANYAMALE, R. J. VERSTEEG, A. WARD, C. STRICKLAND, C. D. JOHNSON, and J. W. LANE, "Use of Electrical Imaging and Distributed Temperature Sensing Methods to Characterize Surface Water–Groundwater Exchange Regulating Uranium Transport at the Hanford 300 Area, Washington," *Water Resources Research*, 46, 10, 1-13 (2010). https://doi.org/10.1029/2010WR009110
3. T. C. JOHNSON, L. D. SLATER, D. NTARLAGIANNIS, F. D. DAY-LEWIS, and M. ELWASEIF, "Monitoring Groundwater-Surface Water Interaction Using Time-Series and Time-Frequency Analysis of Transient Three-Dimensional Electrical Resistivity Changes," *Water Resources Research*, 48, 7 (2012).
4. E. L. WALLIN, T. C. JOHNSON, W. J. GREENWOOD, and J. M. ZACHARA, "Imaging High Stage River-Water Intrusion into a Contaminated Aquifer along a Major River Corridor Using 2-D Time-Lapse Surface Electrical Resistivity Tomography," *Water Resources Research*, 49, 3, 1693-1708 (2013). https://doi.org/10.1002/wrcr.20119
5. T. C. JOHNSON, R. VERSTEEG, J. THOMLE, G. HAMMOND, X. CHEN, and J. ZACHARA, "Four-Dimensional Electrical Conductivity Monitoring of Stage-Driven River Water Intrusion: Accounting for Water Table Effects Using a Transient Mesh Boundary and Conditional Inversion Constraints," *Water Resources Research*, 51, 1-20 (2015). https://doi.org/10.1016/0022-1694(68)90080-2
6. Y. D. FANG, D. APPRIOU, D. H. BACON, V. FREEDMAN, M. L. ROCKHOLD, C. RUPRECHT, G. D. TARTAKOVSKY, M. D. WHITE, S. K. WHITE, and F. ZHANG, *ESTOMP Online User Guide*, Pacific Northwest National Laboratory, Richland, WA (2015). https://stomp-userguide.pnnl.gov/estomp_guide/eSTOMP_guide.stm
7. M. D. WHITE and M. OOSTROM, *STOMP Subsurface Transport Over Multiple Phases, Version 4: User's Guide,* PNNL-15782 (UC-2010), Pacific Northwest National Laboratory, Richland, WA (2006). https://stomp.pnl.gov
8. T. C. JOHNSON, *E4D: A Distributed Memory Parallel Electrical Geophysical Modeling and Inversion Code User Guide - Version 1.0*, PNNL-SA-23783, Pacific Northwest National Laboratory, Richland, WA (2014).
9. T. C. JOHNSON, R. J. VERSTEEG, A. WARD, F. D. DAY-LEWIS, and A. REVIL, "Improved Hydrogeophysical Characterization and Monitoring through Parallel Modeling and Inversion of Time-Domain Resistivity and Induced-Polarization Data," *Geophysics*, 75, 4 (2010).
10. T. C. JOHNSON, G. E. HAMMOND, and X. CHEN. 2017. "PFLOTRAN-E4D: A Parallel Open Source PFLOTRAN Module for Simulating Time-Lapse Electrical Resistivity Data." *Computers and Geosciences* 99, February 2017, 72-80 (2017). https://doi.org/10.1016/j.cageo.2016.09.006
11. CHPRC, *Central Plateau Vadose Zone Geoframework*, ECF-HANFORD-18-0035, Rev. 1, CH2M Hill Plateau Remediation Company, Richland, WA (2019).
12. CHPRC, *Development of the Hanford South Geologic Framework Model, Hanford Site, Washington*, ECF-HANFORD-13-0029, Rev. 5, CH2M Hill Plateau Remediation Company, Richland, WA (2018a).
13. CHPRC, *Model Package Report: Central Plateau Vadose Zone Geoframework*, CP-60925, Rev. 0, CH2M Hill Plateau Remediation Company, Richland, WA (2018b).

14. T. J. BUDGE, *Model Package Report: Central Plateau Groundwater Model, Version 8.2*, CP-57037, Rev. 1, U.S. Department of Energy, Office of Environmental Management, Washington, D.C. (2019).
15. J. ROBINSON, T. C. JOHNSON, J. THOMLE, and I. DEMIRKANLI, *Electrical Resistivity Tomography of the 216-U-1&2 and 216-U-16 WA-1 Waste Sites*, PNNL-30000, Pacific Northwest National Laboratory, Richland, WA (2020).
16. G. V. LAST, E. J. FREEMAN, K. J. CANTRELL, M. J. FAYER, G. W. GEE, W. E. NICHOLS, B. N. BJORNSTAD, and D. G. HORTON, *Vadose Zone Hydrogeology Data Package for Hanford Assessments*, PNNL-14702, Rev. 1, Pacific Northwest National Laboratory, Richland, WA (2006).
17. G. E. ARCHIE, "The Electrical Resistivity Log as an Aid in Determining Some Reservoir Characteristics," *Petroleum Transactions of AIME*, 146, 54-62 (1942).
18. WZ YUE, "Pore-scale Explanation of the Archie's Cementation Exponent: Microstructure, Electrical Anisotropy and Numerical Experiments," *Geophysical Research Letters* 46: 9 (2019). https://doi.org/10.1029/2019GL082585
19. Q. NIU and C ZHANG, "Physical Explanation of Archie's Porosity Exponent in Granular Materials: A Process-Based, Pore-Scale Numerical Study," *Geophysical Research Letters*, 45, 4, 1870-1877 (2018). https://doi.org/10.1002/2017GL076751
20. D. P. LESMES and S. P. FRIEDMAN, "Relationships between the Electrical and Hydrogeological Properties of Rocks and Soils," in *Hydrogeophysics*, 87-128, Springer Netherlands (2005). https://doi.org/10.1007/1-4020-3102-5_4
21. J. ROBINSON, T JOHNSON, and M ROCKHOLD, "Feasibility Assessment of Long-term Electrical Resistivity Monitoring of a Nitrate Plume." *Groundwater*, April, gwat.12899 (2019). https://doi.org/10.1111/gwat.12899.
22. P. BRUNET, R. CLÉMENT, and C. BOUVIER, "Monitoring Soil Water Content and Deficit Using Electrical Resistivity Tomography (ERT) – A Case Study in the Cevennes Area, France," *Journal of Hydrology*, 380, 1–2, 146-53 (2010). https://doi.org/10.1016/j.jhydrol.2009.10.032
23. F. D. DAY-LEWIS, K. SINGHA, and A. M. BINLEY, "Applying Petrophysical Models to Radar Travel Time and Electrical Resistivity Tomograms: Resolution-Dependent Limitations," *Journal of Geophysical Research B: Solid Earth* 110, 8, 1–17 (2005). https://doi.org/10.1029/2004JB003569
24. M. OOSTROM, M. J. TRUEX, M. L. ROCKHOLD, and T. C. JOHNSON, "Deep Vadose Zone Contaminant Flux Evaluation at the Hanford BY-Cribs Site Using Forward and Imposed Concentration Modeling Approaches," *Environmental Processes*, 4, 4, 771-797 (2017). https://doi.org/10.1007/s40710-017-0272-5
25. T. C. JOHNSON and D. M. WELLMAN, *Re-Inversion of Surface Electrical Resistivity Tomography Data from the Hanford Site B-Complex*, PNNL-22520, Pacific Northwest National Laboratory, Richland, WA (2013).
26. T. C. JOHNSON and D. WELLMAN, "Accurate Modelling and Inversion of Electrical Resistivity Data in the Presence of Metallic Infrastructure with Known Location and Dimension," *Geophysical Journal International* 202, 2, 1096–1108 (2015). https://doi.org/10.1093/gji/ggv206
27. D. PARASNIS, "Reciprocity theorems in geoelectric and geoelectromagnetic work," *Geoexploration*, 25, 3, 177-198 (1988).
28. A. KEMNA, "Tomographic Inversion of Complex Resistivity – Theory and applications," PhD Thesis, Bochum Rurh-Iniv., Germany (published by Der Andere Verlag, Osnabruck, Germany) (2000).

ACKNOWLEDGEMENTS
This document was prepared under the Deep Vadose Zone – Applied Field Research Initiative at Pacific Northwest National Laboratory. Funding for this work was provided by the U.S. Department of Energy (DOE) Office of Environmental Management Technology Development. The Pacific Northwest National Laboratory is operated by Battelle Memorial Institute for the DOE under Contract DE-AC05-76RL01830.